SRTTU

Journal of Electrical and Computer Engineering Innovations (JECEI)

Journal homepage: http://www.jecei.sru.ac.ir

JECEI

Research paper

Model Predictive Control of Linear Induction Motor Drive with End Effect Consideration

P. Hamedani [1,*], ***S. Sadr***[2]

[1]*Department of Railway Engineering and Transportation Planning, University of Isfahan, Isfahan, Iran.*

[2]*Department of Electrical Engineering, Tafresh University, Tafresh, Iran.*

Article Info

Article History:
Received 28 June 2022
Reviewed 29 July 2022
Revised 01 August 2022
Accepted 22 October 2022

Keywords:
Linear Induction Motor (LIM)
Electrical motor drive
End Effect
Model Predictive Control (MPC)
Delay compensation
Indirect field oriented control

*Corresponding Author's Email Address:
p.hamedani@eng.ui.ac.ir

Abstract

Background and Objectives: Linear Induction Motors (LIMs) are favorite machines utilized in various industrial applications. But, due to the end effect phenomena, control of a LIM drive is more complicated than rotational machine drives. Therefore, selecting the proper control strategy for a LIM drive has been a significant challenge for the researchers.
Methods: This paper concentrates on a new Model Predictive Control (MPC) of LIM drives which considers the end effect.
Accordingly, the discrete-time model of the LIM with end effect is extracted, and the required flowchart used for the MPC of LIM drive has been presented in this paper.
Results: To study the effectiveness of the suggested strategy, simulation results of a LIM drive with MPC are presented and compared to the traditional Indirect Field Oriented Control (IFOC) of LIM drive. Simulations have been carried out using Matlab. The end effect has been considered in the LIM model and control strategies.
Conclusion: Simulation results validate that the suggested MPC of LIM drive yields excellent dynamic characteristics such as fast speed response with no overshoot. Moreover, in comparison to the traditional IFOC method, the suggested MPC strategy offers lower current ripple and lower electromagnetic force ripple, and therefore, it is suitable for industrial drive applications.

Introduction

Linear electrical motors, including linear induction motors and linear synchronous motors (LSM), are popular machine types in different industries like electrical railway applications [1]-[12]. Linear induction machines, in comparison to synchronous counterparts, have a simple and robust structure, lower cost and maintenance, and self-starting thrust. These advantages make LIMs more prominent in industrial applications than SIMs [12].

However, speed control of LIMs has more difficulties than SIMs [13]-[15]. Until now, different control strategies have been utilized for rotational induction motors, which can also be extended to LIMs, such as [16]-[17]:

- Scalar control methods, for example constant V/f method
- Field Oriented Control (FOC) methods
- Direct Torque Control (DTC) technique
- MPC

FOC and DTC have been used in many industrial and domestic applications. However, they have some issues. To overcome these issues, new variations have been proposed, which usually complicate the implementation of the control strategy in practice [18]. In the past decade, with the development of digital signal processors (DSPs), MPC has been proposed as an interesting solution [18]-[19].

MPC approach needs the mathematical model of the system for predicting variables. A selected cost function is calculated for all possible switching states in each sampling time. Finally, the optimal switching states that minimize the cost function are chosen for firing the inverter switches in the next sampling time [18]-[21]. The main benefits of MPC are simple implementation and nonlinear solutions [18]-[20].

Although the PMC strategy has been a very popular control strategy for different electrical motor drives [22]-[23], in the case of LIMs, only a few works have been done until now [24]. In [25] and [26], MPC of LIM drive has been reported. But in these papers, the end effect has been counted in the direct axis circuit model and in the quadrature axis circuit model, the end effect is not considered. But, to accurately model a LIM, the end effect should be taken into account in both d- and q-axis equivalent circuits [27]-[28]. Moreover, in [25] and [26], the delay compensation method has not been studied in the MPC algorithm. By applying the delay compensation method, delay time that arises because of the large number of calculations will be compensated and the current ripple will be improved [30].

Consequently, this paper aims to investigate a new strategy for predictive control of the LIM drive considering the end effect. To reduce the computational time delay, a delay compensation methodology is used in the MPC of the LIM drive. Moreover, in this work, MPC and IFOC of the LIM drive are discussed from their basic theoretical concepts. The performance of these strategies is compared under transient and steady-state conditions. The same parameters and operating conditions have been considered for both approaches to guarantee a fair comparison.

The following sections of the paper will present the MPC strategy (including the discrete-time model of LIM and the MPC algorithm of LIM drive), the IFOC strategy (including the dynamic model of LIM and the vector control method of LIM drive), results, and the conclusion.

Discrete-time Model of the LIM with End Effect

In a three-phase LIM, the primary voltage equation can be written as follows:

$$\mathbf{V}_s = \mathbf{R}_s \mathbf{i}_s + \mathbf{L}_s \frac{d\boldsymbol{\psi}_s}{dt} \tag{1}$$

Table 1 provides the notation for parameters and variables used in this paper.

The primary and secondary flux equations can be expressed as [21]:

$$\boldsymbol{\psi}_s = \mathbf{L}_s \mathbf{i}_s + \mathbf{L}_m \mathbf{i}_r \tag{2}$$

$$\boldsymbol{\psi}_r = \mathbf{L}_r \mathbf{i}_r + \mathbf{L}_m \mathbf{i}_s \tag{3}$$

Table 1: Notation for parameters and variables

symbol	Description
$\mathbf{V_s}$	Primary voltage vector
$\mathbf{i_s}$	Primary current vector
$\boldsymbol{\psi_s}$	Primary flux vector
$\mathbf{R_s}$	Primary resistance matrix
$\mathbf{L_s}$	Primary inductance matrix
$\mathbf{i_r}$	Secondary current vector
$\boldsymbol{\psi_r}$	Secondary flux vector
$\mathbf{L_r}$	Secondary inductance matrix
$\mathbf{L_m}$	Magnetizing inductance matrix
F	Electromagnetic force
τ	Motor pole pitch
k	Sampling instant
T_s	Sampling time
R_s	Primary resistance
L_s	Primary inductance
R_r	Secondary resistance
L_r	Secondary inductance
L_m	Magnetizing inductance
L_{m_0}	Magnetizing inductance at zero speed
D	Motor length
V_r	Motor speed
λ_ψ	Weighting factor in cost function
ω_r	Angular velocity of LIM
ω_e	Angular velocity of reference frame
λ_{dr}	d-axis secondary flux

The electromagnetic force can be described as [28]:

$$F = \frac{3}{2}\frac{\pi}{\tau}\operatorname{Im}\{\overline{\boldsymbol{\psi}}_s \mathbf{i}_s\} \tag{4}$$

in which $\overline{\boldsymbol{\psi}}_s$ is the complex conjugate value of $\boldsymbol{\psi}_s$.

The discrete-time model of the LIM can be calculated from (1)-(2) using the Euler forward approximation [21]:

$$\boldsymbol{\psi}_s(k+1) = \boldsymbol{\psi}_s(k) + T_s \mathbf{V}_s(k) - R_s T_s \mathbf{i}_s(k) \tag{5}$$

$$\boldsymbol{\psi}_r(k+1) = \frac{L_r}{L_s}\boldsymbol{\psi}_s(k+1) + \mathbf{i}_s(k)\left(L_m - \frac{L_r L_s}{L_m}\right) \tag{6}$$

$$\mathbf{i}_s(k+1) = \left(1 - \frac{T_s}{\tau_\sigma}\right)\mathbf{i}_s(k) + \frac{T_s}{\tau_\sigma}\left\{\frac{1}{R_\sigma}\left[\left(\frac{K_r}{\tau_r} - jK_r\omega_r\right)\boldsymbol{\psi}_r(k+1) + \mathbf{V}_s(k)\right]\right\} \tag{7}$$

$$F(k+1) = \frac{3}{2}\frac{\pi}{\tau}\operatorname{Im}\{\overline{\boldsymbol{\psi}}_s(k+1)\mathbf{i}_s(k+1)\} \tag{8}$$

in which $R_\sigma = R_s + R_r K_r^2$, $K_r = \frac{L_m}{L_r}$, $\sigma = 1 - \frac{L_m^2}{L_s L_r}$,

$$\tau_\sigma = \frac{\sigma L_s}{R_\sigma} \tag{9}$$

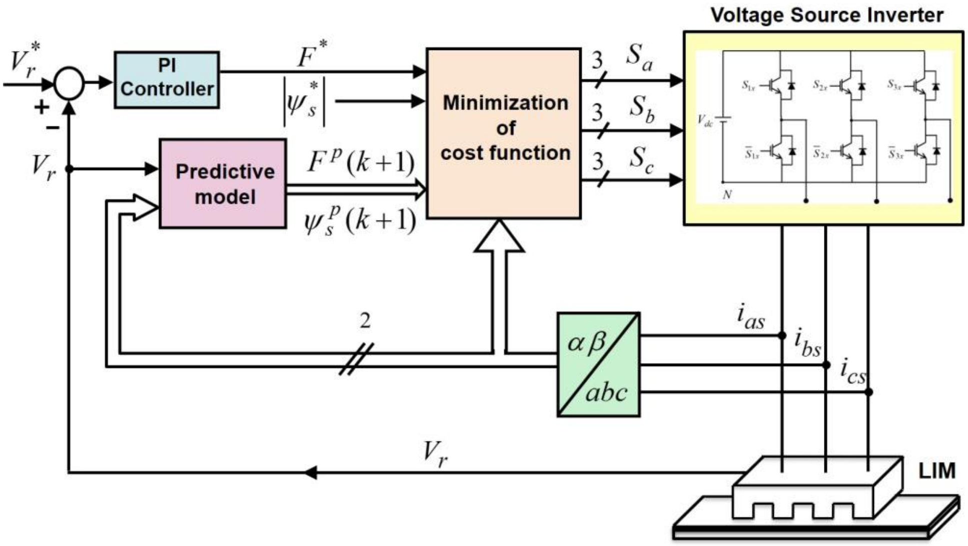

Fig. 1: Block diagram of MPC for the LIM drive.

To consider the end effect in the LIM model, the magnetizing inductance must be modified according to Duncan's model [28]:

$$L_m = L_{m_0}\left(1 - f(Q)\right) \tag{10}$$

where

$$f(Q) = \left(1 - e^{-Q}\right)/Q\,,\quad Q \cong \frac{D.\,R_r}{L_r.V_r} \tag{11}$$

Model Predictive Control of LIM drive

Model predictive control of the LIM drive is performed in the α-β stationary reference frame. Therefore, Clark's transformation is utilized to convert a, b, and c primary voltage and currents to α and β primary voltage and currents [30]:

$$\begin{bmatrix} f_\alpha \\ f_\beta \end{bmatrix} = \frac{2}{3}\begin{bmatrix} 1 & -\frac{1}{2} & -\frac{1}{2} \\ 0 & \frac{\sqrt{3}}{2} & -\frac{\sqrt{3}}{2} \end{bmatrix}\begin{bmatrix} f_a \\ f_b \\ f_c \end{bmatrix} \tag{12}$$

$$\mathbf{V}_s = V_\alpha + jV_\beta \quad , \ \mathbf{i}_s = i_\alpha + j\,i_\beta \tag{13}$$

in which *f* donates the voltage or current variables.

Fig. 1 illustrates the diagram of the MPC-based LIM drive. A discrete PI controller with unti-windup produces the reference force, *F**. The MPC diagram calculates the future values of primary flux and force utilizing (5)-(8). The predicted and command values of the primary flux and force are compared in a cost function. All possible switching conditions are considered. In a 2-level voltage source inverter, eight various switching combinations happen. The one that minimizes the cost function is selected as the next switching condition applied to the inverter.

The cost function is considered as follows:

$$g = \left|F^* - F(k+1)\right| + \lambda_\psi \left|\boldsymbol{\psi}_s^* - \boldsymbol{\psi}_s(k+1)\right| \tag{14}$$

The weighting factor is considered as the ratio of the rated force and rated stator flux:

$$\lambda_\psi = \frac{F_n}{2\left|\psi_{s_n}\right|} \tag{15}$$

To moderate the time delay that arises because of the high number of computations, the delay compensation methodology has been proposed [30]. This method calculates the predicted values in the next shifted forward sample time [30]:

$$\boldsymbol{\psi}_s(k+2) = \boldsymbol{\psi}_s(k+1) + T_s\,\mathbf{V}_s(k+1) - R_s\,T_s\,\mathbf{i}_s(k+1) \tag{16}$$

$$\boldsymbol{\psi}_r(k+2) = \frac{L_r}{L_s}\boldsymbol{\psi}_s(k+2) + \mathbf{i}_s(k+1)\left(L_m - \frac{L_r\,L_s}{L_m}\right) \tag{17}$$

$$\mathbf{i}_s(k+2) = \left(1 - \frac{T_s}{\tau_\sigma}\right)\mathbf{i}_s(k+1) + \frac{T_s}{\tau_\sigma}\left\{\frac{1}{R_\sigma}\left[\left(\frac{K_r}{\tau_r} - j\,K_r\,\omega_r\right)\boldsymbol{\psi}_r(k+2) + \mathbf{V}_s(k+1)\right]\right\} \tag{18}$$

$$F(k+2) = \frac{3}{2}\frac{\pi}{\tau}\mathrm{Im}\left\{\overline{\boldsymbol{\psi}}_s(k+2)\,\mathbf{i}_s(k+2)\right\} \tag{19}$$

Consequently, the cost function can be written as:

$$g = \left|F^* - F(k+2)\right| + \lambda_\psi\left|\boldsymbol{\psi}_s^* - \boldsymbol{\psi}_s(k+2)\right| \tag{20}$$

Fig. 2 shows the flowchart for the MPC for LIM drive with delay compensation.

Dynamic Model of the LIM with End Effect

IFOC of the LIM drive is performed in the q-d synchronous rotational reference frame. Therefore, Park's transformation is utilized to convert a, b, and c variables to the q and d variables. Primary and secondary voltage equations are written as [29]:

$$v_{qs} = R_s i_{qs} + \omega_e\,\lambda_{ds} + p\lambda_{qs} \tag{21}$$

$$v_{ds} = R_s i_{ds} - \omega_e\,\lambda_{qs} + p\lambda_{ds} \tag{22}$$

$$v_{qr} = R_r i_{qr} + (\omega_e - \omega_r)\lambda_{dr} + p\lambda_{qr} = 0 \quad (23)$$

$$v_{dr} = R_r i_{dr} - (\omega_e - \omega_r)\lambda_{qr} + p\lambda_{dr} = 0 \quad (24)$$

Primary and secondary flux linkage equations are written as [29]:

$$\lambda_{qs} = L_{ls} i_{qs} + L_m\{1 - f(Q)\}(i_{qs} + i_{qr}) \quad (25)$$

$$\lambda_{ds} = L_{ls} i_{ds} + L_m\{1 - f(Q)\}(i_{ds} + i_{dr}) \quad (26)$$

$$\lambda_{qr} = L_{lr} i_{qr} + L_m\{1 - f(Q)\}(i_{qs} + i_{qr}) \quad (27)$$

$$\lambda_{dr} = L_{lr} i_{dr} + L_m\{1 - f(Q)\}(i_{ds} + i_{dr}) \quad (28)$$

where $p \equiv d/dt$.

The LIM thrust can be written as:

$$F = \frac{3}{2}\frac{\pi}{\tau}\left(\lambda_{qr} i_{dr} - \lambda_{dr} i_{qr}\right) \quad (29)$$

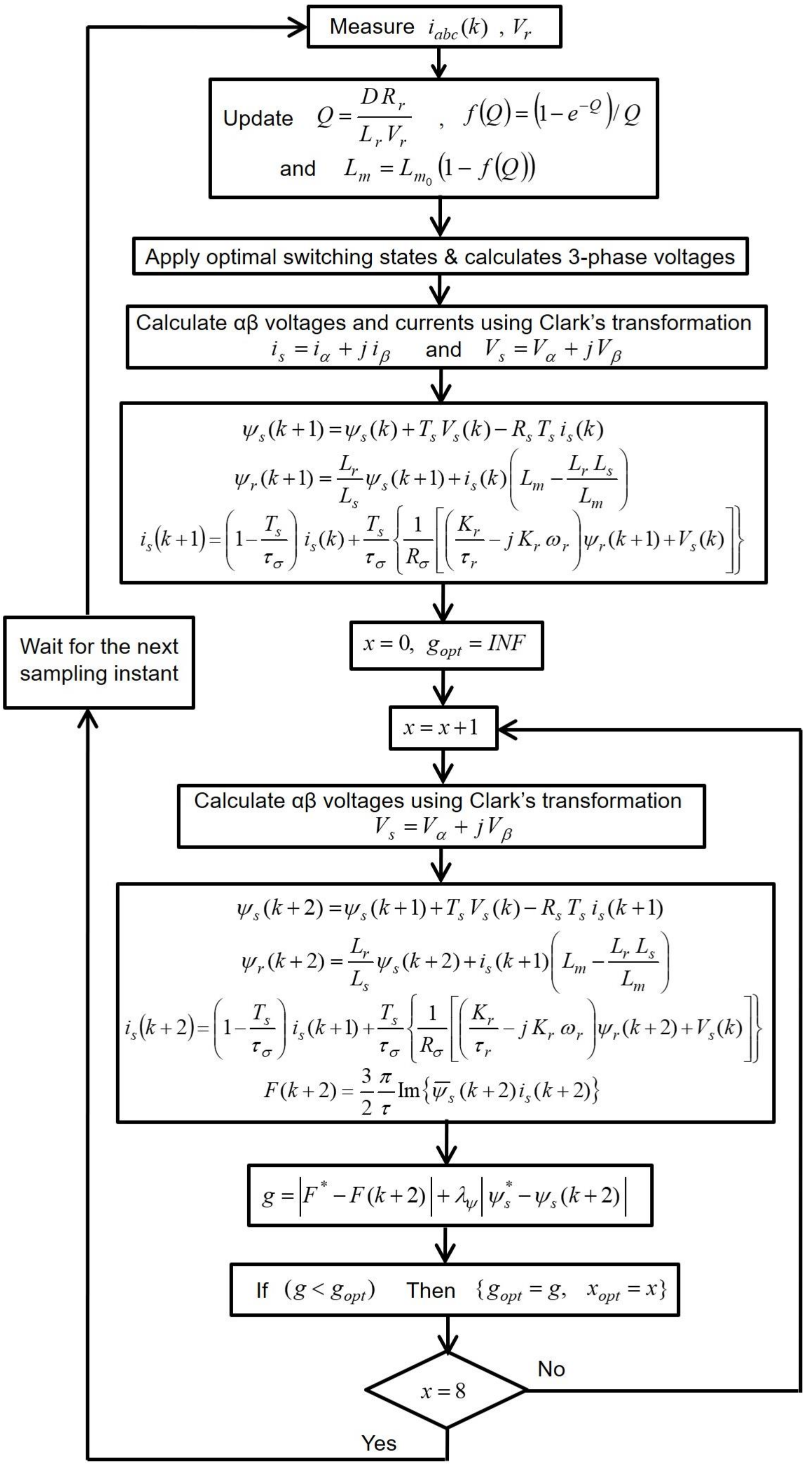

Fig. 2: Flowchart for MPC of the LIM drive.

IFOC of LIM Drive

Fig. 3 shows the IFOC diagram for the LIM drive. To decouple the flux and the LIM force, the below assumption is made in this strategy [28]:

$$\lambda_{qr} = 0 \quad , \quad \frac{d\lambda_{qr}}{dt} = 0 \tag{30}$$

As a result and by supposing $v_{qr} = v_{dr} = 0$, the slip frequency ($\omega_{sl} \equiv \omega_e - \omega_r$), λ_{dr}, and the LIM force can be computed as [28]:

$$\omega_{sl} = R_r \left[\frac{1 - f(Q)}{\frac{L_{lr}}{L_m} + (1 - f(Q))} \right] \times \frac{i_{qs}}{\lambda_{dr}} \tag{31}$$

$$\lambda_{dr} = \frac{L_m (1 - f(Q))}{1 + \left\{ \frac{L_{lr} + L_m (1 - f(Q))}{R_r} \right\} p} \times i_{ds} \tag{32}$$

$$F = \frac{3}{2} \frac{\pi}{\tau} \frac{L_m (1 - f(Q))}{L_{lr} + L_m (1 - f(Q))} \lambda_{dr} i_{qs} \tag{33}$$

The IFOC scheme is composed of two control loops. The outer loop controls the LIM speed using a PI controller and generates the reference q-axis current (i_{qs}^*). The inner loop controls the LIM phase currents using a hysteresis controller and produces the switching pulses of the inverter.

The slip frequency (ω_{sl}) and the reference d-axis current (i_{ds}^*) are generated using (31) and (32), respectively.

As shown in Fig. 3, ω_{sl} and i_{ds}^* are calculated using gains K_1 and K_2 which depend on the end effect and machine velocity.

Results and Discussion

To investigate the effectiveness of the MPC of LIM drive with end effect, simulation results are provided in this section. The end effect is considered in the LIM model and MPC strategy. Moreover, the results are compared with the IFOC of LIM drive with the end effect. Simulations are implemented using Matlab. In both methods, the same parameters and conditions have been used for the simulations. Table 2 shows the simulation parameters. The utilized gains in the PI controller are $K_i = K_p = 50$.

Table 2: Simulation Parameters of LIM drive.

Phase voltage	220 V	R_r	0.843 Ω
Nominal current	93.65 A	L_s	4.5 mH
Power factor	0.4884	L_m	3 mH
Poles	4	L_r	3.1 mH
τ	0.1024 m	λ^*_{dr}	0.24 Wb
D	0.413 m	M	29.34 kg
R_s	0.049 Ω	Rated Load	879 N

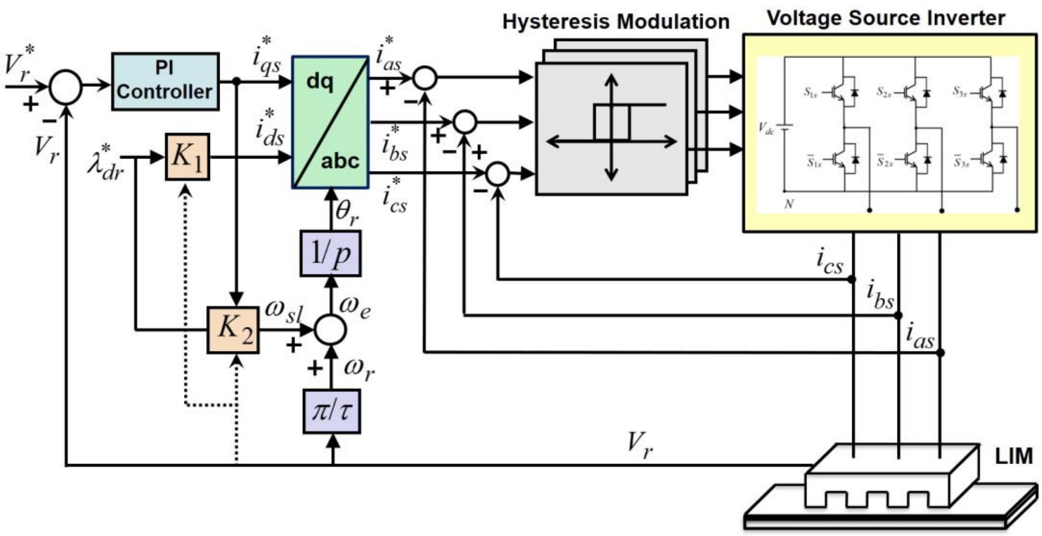

Fig. 3: Block diagram of IFOC for the LIM drive.

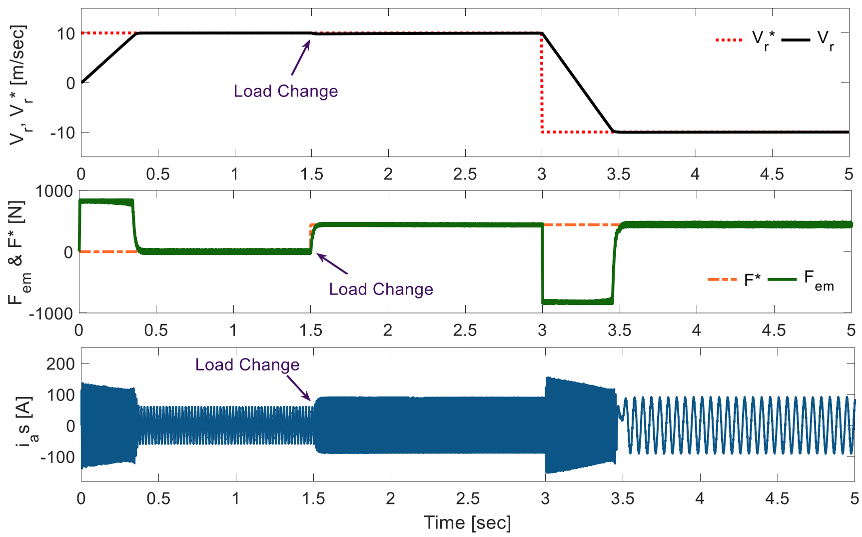

Fig. 4: Speed response, electromagnetic force response, and phase current LIM drive with MPC method.

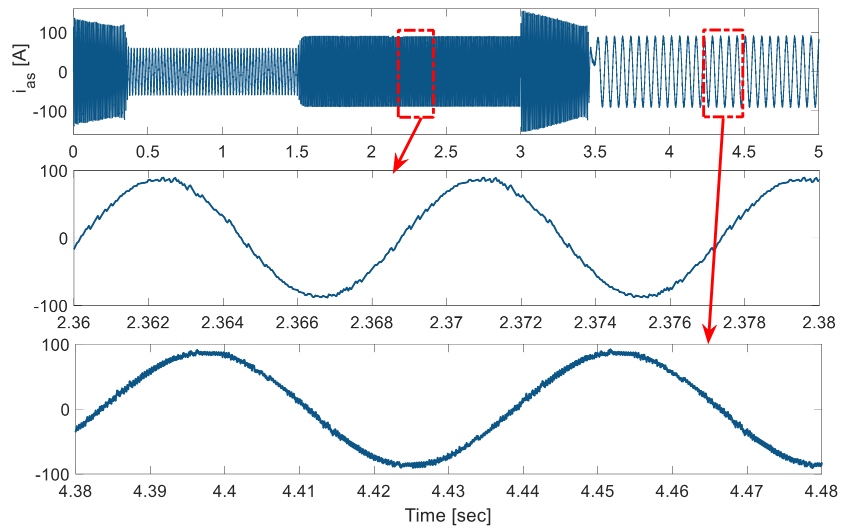

Fig. 5: Phase current ripple of LIM drive with MPC method.

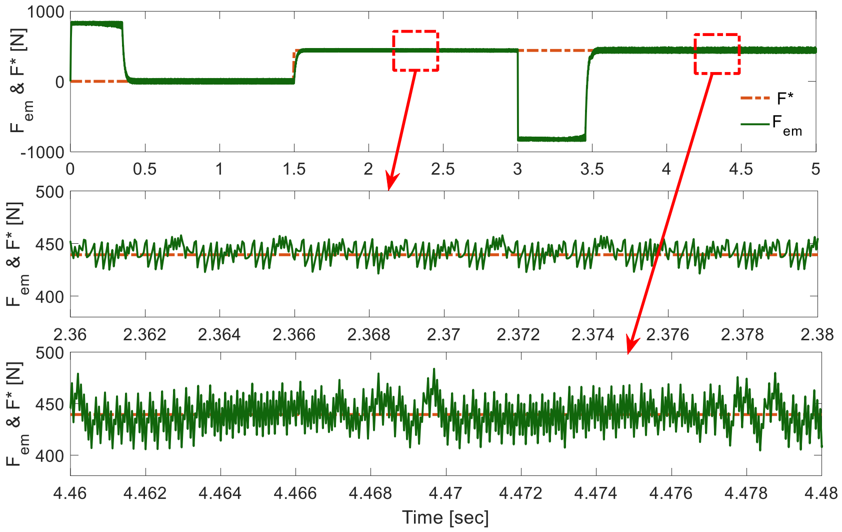

Fig. 6: Electromagnetic force ripple of LIM drive with MPC method.

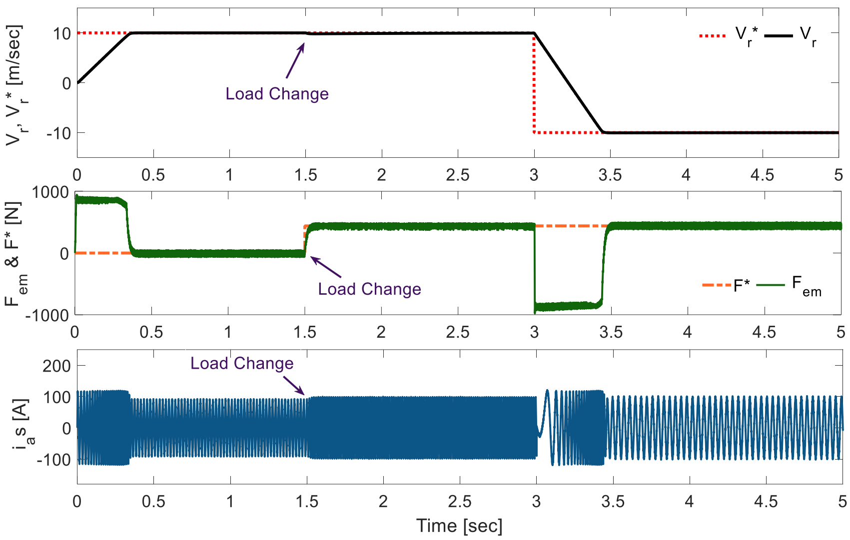

Fig. 7: Speed response, electromagnetic force response, and phase current of LIM drive with IFOC.

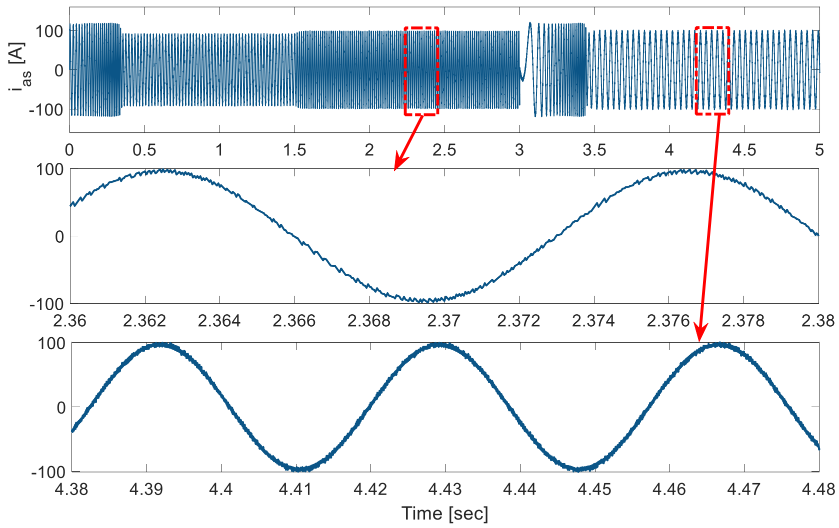

Fig. 8: Phase current ripple of LIM drive with IFOC method.

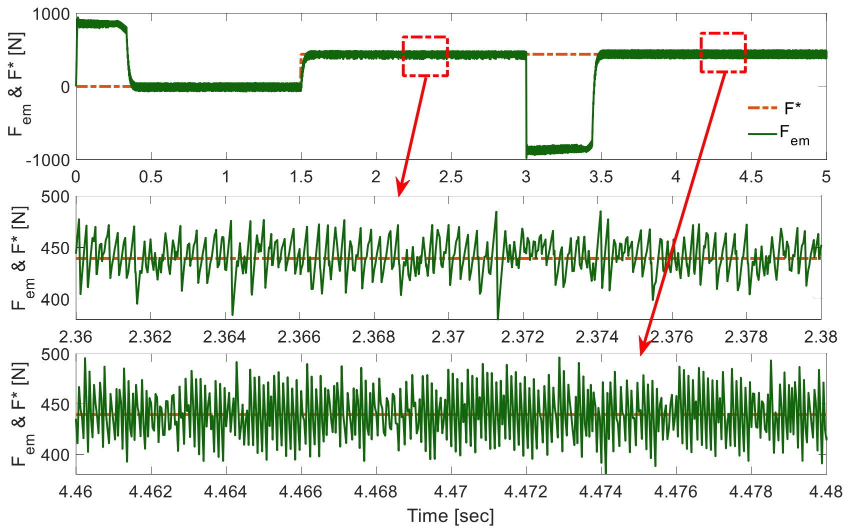

Fig. 9: Electromagnetic force ripple of LIM drive with IFOC method.

At the start, a reference speed equal to 10 m/sec is applied, and it changes to -10 m/sec at t=3 sec. The LIM drive starts in no-load condition, and an external load is applied to the machine at t=1.5 sec. For the IFOC method, the hysteresis band has been taken equal to 0.5 A.

Fig. 4 illustrates the speed, electromagnetic force, and phase current of the LIM drive with the MPC method, respectively. Clearly, the actual LIM speed follows the reference speed in motoring and braking conditions. Fig. 5 shows the phase current ripple of the LIM drive with the MPC method. Fig. 6 represents the electromagnetic force ripple of the LIM drive with MPC method.

According to Fig. 6, the LIM force tracks the external load in motoring and braking conditions.

Fig. 7 compares the speed, electromagnetic force, and phase current of the LIM drive with the IFOC method, respectively. Like the case of the MPC method, in the IFOC strategy, the actual LIM speed tracks the reference speed in motoring and braking conditions. Fig. 8 shows the phase current ripple of the LIM drive with the IFOC method. Fig. 9 represents the electromagnetic force ripple of the LIM drive with the IFOC method.

Comparison of Fig. 4 with Fig. 7 manifest that both methods yield similar dynamic performance in the speed response. However, a comparison of Fig. 5 with Fig. 8 shows that the MPC method has a lower current ripple. Moreover, a comparison of Fig. 6 with Fig. 9 demonstrates that the MPC method has a lower electromagnetic force ripple. Table 3 shows the current ripple and force ripple of the MPC and IFOC methods.

Table 3: Comparison of current ripple and force ripple in MPC and IFOC methods of LIM drive.

		IFOC	MPC
Current ripple	V_r^* = 10 m/sec	3 A	2.5 A
	V_r^* = -10 m/sec	5 A	3.5 A
Force ripple	V_r^* = 10 m/sec	48 A	22 A
	V_r^* = -10 m/sec	60 A	46 A

Conclusion

This work proposes the MPC strategy for LIM drives, considering the end effect. The discrete-time model of the LIM with end effect has been extracted, and the required flowchart utilized for the model predictive control of LIM drive has been presented. To evaluate the accuracy of the suggested strategy, MPC is compared to the traditional IFOC for the LIM drive.

Simulation results manifest that the suggested model predictive control of LIM drive achieves perfect dynamic characteristics such as fast speed response with no overshoot. In addition, compared to the traditional indirect field-oriented control, the proposed model predictive control offers lower current ripple and lower electromagnetic force ripple.

Author Contributions

P. Hamedani carried out the simulation results. S. Sadr interpreted the results. P. Hamedani and S. Sadr wrote the manuscript.

Acknowledgment

The authors thankfully appreciate the anonymous reviewers and the editor of JECEI for their useful comments and suggestions.

Conflict of Interest

The authors declare no potential conflict of interest regarding the publication of this work. In addition, the ethical issues including plagiarism, informed consent, misconduct, data fabrication and, or falsification, double publication and, or submission, and redundancy have been completely witnessed by the authors.

Abbreviations

LIM	Linear Induction Motor
LSM	Linear Synchronous Motor
MPC	Model Predictive Control
IFOC	Indirect Field Oriented Control
DTC	Direct Torque Control
VSI	Voltage Source Inverter

References

[1] A. Shiri, A. Shoulaie, “End effect braking force reduction in high-speed single-sided linear induction machine,” Int. J. Energy Convers. Manage., 61: 43-50, 2012.

[2] X. Qiwei, S. Cui, Q. Zhang, L. Song, X. Li, "Research on a new accurate thrust control strategy for linear induction motor," IEEE Trans. Plasma Sci., 43(5): 1321-1325, 2015.

[3] R. Cao, Y. Jin, M. Lu, Z. Zhang, "Quantitative comparison of linear flux-switching permanent magnet motor with linear induction motor for electromagnetic launch system," IEEE Trans. Ind. Electron., 65(9): 7569-7578, 2018.

[4] J. Q. Li, W. L. Li, G. Q. Deng, Z. Ming, "Continuous-behavior and discrete-time combined control for linear induction motor-based urban rail transit," IEEE Trans. Mag., 52(7): 1-4, 2016.

[5] T. Wang, B. Li, B. Xie, F. Fang, "Linear induction motors for driving vehicles climbing on steel plates," IEEE Trans. Energy Convers., 29(3): 788-789, 2014.

[6] J. Lim, J. H. Jeong, C. H. Kim, C. W. Ha, D. Y. Park, "Analysis and experimental evaluation of normal force of linear induction motor for maglev vehicle," IEEE Trans. Magn., 53(11): 1-4, 2017.

[7] R. Cao, M. Lu, N. Jiang, M. Cheng, "Comparison between linear induction motor and linear flux-switching permanent-magnet motor for railway transportation," IEEE Trans. Ind. Electron., 66(12): 9394-9405, 2019.

[8] W. Y. Ji, G. Jeong, C. B. Park, I. H. Jo, H. W. Lee, "A study of non-symmetric double-sided linear induction motor for hyperloop all-in-one system (Propulsion, Levitation, and Guidance)," IEEE Trans. Magn., 54(11): 1-4, 2018.

[9] M. Shujun, C. Jianyun, S. Xudong, W. Shanming, "A variable pole pitch linear induction motor for electromagnetic aircraft launch system," IEEE Trans. Plasma Sci., 43(5): 1346-1351, 2015.

[10] H. Seo, J. Lim, G. H. Choe, J. Y. Choi, J. H. Jeong, "Algorithm of linear induction motor control for low normal force of magnetic levitation train propulsion system," IEEE Trans. Magn., 54(11): 1-4, 2018.

[11] H. Karimi, S. Vaez-Zadeh, F. Rajaei Salmasi, "Combined vector and direct thrust control of linear induction motors with end effect compensation," IEEE Trans. Energy Convers., 31(1): 196-205, 2016.

[12] P. Hamedani, S. Sadr, A. Shoulaie "Independent fuzzy logic control of two five-phase linear induction motors supplied from a single voltage source inverter," J. Electr. Comput. Eng. Innovations (JECEI), 10(1): 195-208, 2021.

[13] K. Wang, Y. Li, Q. Ge, L. Shi, "An improved indirect field-oriented control scheme for linear induction motor traction drives," IEEE Trans. Ind. Electron., 65(12): 9928-9937, 2018.

[14] D. Hu, W. Xu, R. Dian, Y. Liu, J. Zhu, "Loss minimization control of linear induction motor drive for linear metros," IEEE Trans. Ind. Electron., 65(9), 6870-6880, 2018.

[15] A. Accetta, M. Cirrincione, M. Pucci, A. Sferlazza, "State space-vector model of linear induction motors including end-effects and iron losses part i: theoretical analysis," IEEE Trans. Ind. Appl., 56(1), 235-244, 2020.

[16] A. Poorfakhraei, M. Narimani, A. Emadi, "A review of modulation and control techniques for multilevel inverters in traction applications," IEEE Access, 9: 24187–24204, 2021.

[17] A. Poorfakhraei, M. Narimani, A. Emadi, "A review of multilevel inverter topologies in electric vehicles: current status and future trends," IEEE Open J. Power Electron., 2: 155–170, 2021.

[18] F. Wang, Z. Zhang, X. Mei, J. Rodríguez, R.; Kennel, "Advanced control strategies of induction machine: field oriented control, direct torque control and model predictive control," Energies, 11(1): 1-13, 2018.

[19] J. Rodriguez, R. Kennel, J. R. Espinoza, M. Trincado, C. A. Silva, C. A. Rojas, "High-Performance Control Strategies for Electrical Drives: An Experimental Assessment," IEEE Trans. Ind. Electron., 59(2), 812–820, 2012.

[20] M. Rivera, J. Rodriguez, S. Vazquez, "Predictive control in power converters and electrical drives—part I," IEEE Trans. Ind. Electron., 63(6): 3834-3836, 2016.

[21] J. Rodriguez, P. Cortes, Predictive Control of Power Converters and Electrical Drives, vol. I. Wiley-IEEE Press: 123, 2012.

[22] J. Rodriguez et al., "Latest advances of model predictive control in electrical drives—part i: basic concepts and advanced strategies," IEEE Trans. Power Electron., 37(4): 3927-3942, 2022.

[23] M. F. Elmorshedy, W. Xu, F. F. M. El-Sousy, M. R. Islam, A. A. Ahmed, "Recent achievements in model predictive control techniques for industrial motor: a comprehensive state-of-the-art," IEEE Access, 9: 58170-58191, 2021.

[24] M. F. Elmorshedy, W. Xu, S. M. Allam, J. Rodriguez, C. Garcia, "MTPA-based finite-set model predictive control without weighting factors for linear induction machine," IEEE Trans. Ind. Electron., 68(3): 2034-2047, 2021.

[25] N. J., Merlin Mary, C. Ganguly, M. Kowsalya, "Simulation of linear induction motor using model predictive control in synchronously rotating reference frame," presented at the IEEE 1st International Conference on Power Electronics, Intelligent Control and Energy Systems (ICPEICES), 2016.

[26] S. M. Kazraji, M. B. B. Sharifian, "Model predictive control of linear induction motor drive," presented at the 43rd Annual Conference of the IEEE Industrial Electronics Society (IECON), 2017.

[27] G. Kang, K. Nam, "Field-oriented control scheme for linear induction motor with the end effect," IEE Proc. on Electr. Power Appl., 152(1): 1565-1572, 2005.

[28] P. Hamedani, A.Shoulaie, "Utilization of CHB multilevel inverter for harmonic reduction in fuzzy logic controlled multiphase LIM drives," J. Electr. Comput. Eng. Innovations (JECEI), 8(1): 19-30, 2020.

[29] P. Hamedani, A. Shoulaie, "Modification of the field-weakening control strategy for linear induction motor drives considering the end effect," Adv. Electr. Comput. Eng. (AECE), 15(3): 3-12, 2015.

[30] P. Hamedani, C. Garcia, F. Flores-Bahamonde, S. Sadr, J. Rodriguez, "Predictive control of 4-level flying capacitor inverter for electric car applications," presented at the 13th Power Electronics, Drive Systems, and Technologies Conference (PEDSTC): 224-229, 2022.

Biographies

Pegah Hamedani was born in Isfahan, Iran, in 1985. She received B.Sc. and M.Sc. degrees from University of Isfahan, Iran, in 2007 and 2009, respectively, and the Ph.D. degree from Iran University of Science and Technology, Tehran, in 2016, all in Electrical Engineering. Her research interests include power electronics, control of electrical motor drives, supply system of the electric railway (AC and DC), linear motors & MAGLEVs, and analysis of overhead contact systems. She is currently an Assistant Professor with the Department of Railway Engineering and Transportation Planning, University of Isfahan, Isfahan, Iran. Dr. Hamedani was the recipient of the IEEE 11th Power Electronics, Drive Systems, and Technologies Conference (PEDSTC'20) best paper award in 2020.

- Email: p.hamedani@eng.ui.ac.ir
- ORCID: 0000-0002-5456-1255
- Web of Science Researcher ID: AAN-2662-2021
- Scopus Author ID: 37118674000
- Homepage: https://engold.ui.ac.ir/~p.hamedani/

Sajad Sadr received the B.Sc. degree in electronic engineering from Bu-Ali Sina University, Hamedan, Iran, in 2006, and the M.Sc. degree in electrical engineering from Amirkabir University of Technology, Tehran, Iran, in 2009. Ph.D. degree in electrical engineering from Iran University of Science and Technology, Tehran, Iran, in 2016. He is currently an Assistant Professor with the Department of Electrical Engineering, Tafresh University, Tafresh, Iran. His research interests include power electronics and motor drives.

- Email: sadr@tafreshu.ac.ir
- ORCID: 0000-0002-6113-8930
- Web of Science Researcher ID: GVT-2596-2022
- Scopus Author ID: 56367494300
- Homepage: http://faculty.tafreshu.ac.ir/sadr/fa

How to cite this paper:
P. Hamedani, S. Sadr, "Model predictive control of linear induction motor drive with end effect consideration," J. Electr. Comput. Eng. Innovations, 11(2): 253-262, 2023.

DOI: 10.22061/jecei.2022.9191.586

URL: https://jecei.sru.ac.ir/article_1804.html